Range profiles in self-ion-implanted crystalline Si

K. Nordlund, J. Keinonen, E. Rauhala, and T. Ahlgren
Accelerator Laboratory, University of Helsinki, P.O. Box 43, FIN-00014 Helsinki, Finland
(Received 17 February 1995; revised manuscript received 14 July 1995)

Range profiles of 50- and 100-keV $^{30}Si^{+}$ ions implanted into Si(100) at room temperature with doses from 2×10^{16} to 1×10^{18} ions cm^{-2}, and of 2×10^{16} 50-keV $^{30}Si^{+}$ ions cm^{-2} in Si(100) preimplanted with 50-keV $^{28}Si^{+}$ ions with doses from 5×10^{13} to 1×10^{18} ions cm^{-2}, have been studied with nuclear reaction techniques. The structural transformation of the samples was studied by Rutherford backscattering and channeling. The dependence of the range profile on the damage structure of the sample has been examined by comparing measured range profiles with those obtained in molecular-dynamics simulations. The dependence of the range profile on the polycrystalline sample structure is shown.

I. INTRODUCTION

Ion implantation of crystalline silicon (c-Si) is a key processing technique for precise doping in semiconductor technology. As device sizes in integrated circuits are decreased the need to understand processes that produce damage in c-Si during and after the ion implantation is emphasized. Several techniques have been used to study the detailed structures of the complex ion-implantation-induced defects, for example electron paramagnetic resonance,[1] infrared optical absorption,[2] transmission electron microscopy,[3] optical reflection spectroscopy,[4] x-ray double crystal diffractometry,[5] Raman spectroscopy,[6] slow positron annihilation,[7] and Rutherford backscattering spectrometry (RBS)/ion channeling.[8] An annealing process that occurs during ion irradiation has been reported by many authors to be effective on already existing damage.[7,9,10] As a result silicon surface layers, rendered amorphous by high dose ion implantation have been known to reorder as a polycrystalline network under some implantation conditions.[11,12]

The aim of this study was to continue our work on slowing down and damage formation in self-ion implantation of c-Si.[13–15] Now we focus on the study of slowing down in strongly damaged silicon caused by very high dose implantation. In spite of the fact that the damage structures have been extensively studied in the literature,[6,9,10,16–19] there is to our knowledge no studies on the effect of the damage structure of the sample on the slowing down and range of keV Si ions in ion implanted c-Si.

II. EXPERIMENTAL PROCEDURE

Samples were prepared at the isotope separator of the laboratory by implanting fluences of 2×10^{16} 50-keV $^{30}Si^{+}$ ions cm^{-2}, 1×10^{17} 100-keV $^{30}Si^{+}$ ions cm^{-2}, and 5×10^{13} to 1×10^{18} 50-keV $^{28}Si^{+}$ ions cm^{-2} into n-type Si(100) slices (Czochralski grown, doped uniformly by P to a resistivity of 2.5–3.5 Ω cm) at room temperature. The dose rates used in the implantations varied between 5.7 and 11.2 $\mu A\ cm^{-2}$ for the $^{28}Si^{+}$ implantations and 0.25 and 0.51 $\mu A\ cm^{-2}$ for the $^{30}Si^{+}$ implantations. To prevent sample heating during implantation the back side of the sample was firmly placed against a background copper pedestal which acted as a heat sink. From studies of the heat conduction conditions in the implantation setup we know that the sample does not warm up more than a few degrees K even for the highest-dose implants. During the implantations the specimen normal ([100] crystal axis) was tilted 6° off the beam direction towards the [010] crystal axis.

At doses lower than 10^{16} ions cm^{-2} only $^{28}Si^{+}$ was implanted. At doses higher than 10^{16} ions cm^{-2} the concentration of implanted atoms was high enough to enable the measurement of implanted ^{30}Si distributions by nuclear reaction techniques. Therefore, for such measurements samples were prepared by implanting only with 2×10^{16} 50-keV $^{30}Si^{+}$ ions cm^{-2} or by first irradiating with 2×10^{16} to 1×10^{18} 50-keV $^{28}Si^{+}$ ions cm^{-2} and then with 2×10^{16} 50-keV $^{30}Si^{+}$ ions cm^{-2}.

To probe the ^{30}Si range distributions in the samples, the nuclear-resonance-broadening (NRB) technique was used,[20] along with the sharp [Γ = 68 eV (Ref. 21)], strong [S=5 eV (Ref. 21)], and isolated resonance of the $^{30}Si(p,\gamma)^{31}P$ reaction at E_p = 620 keV. The proton beams of about 1 μA were supplied by the 2.5 MV Van de Graaff accelerator of the laboratory. The resolving power of the beam, typically 400 eV, was determined at the 620 keV resonance with an unimplanted c-Si sample containing 3.1 at. % of the isotope ^{30}Si. It corresponds to the depth resolution of about 5 nm at the surface. The beam was focused to a spot of 3×3 mm^2. Effects associated with the probing proton beam were controlled by repeating each measurement twice at each beam spot. The γ radiation was detected in a 12.7 cm (diameter) ×10.2 cm NaI(Tl) crystal shielded against the background radiation by 5 cm of lead.

The crystallinity of the implanted samples was determined by RBS and channeling of 2.0-MeV $^{4}He^{+}$ ions from the 2.5 MV Van de Graaff accelerator of the laboratory. The angular divergence of the incident beam was less than 0.02°. Backscattered particles were analyzed with a 50 mm^2 Si(Li) detector located at 155° with respect to the incident beam at a distance of 65 mm from the target. The resolution of the detector was 16 keV for the backscattered α particles. The samples were mounted on a precision goniometer, and the beam was aligned with respect to the ⟨100⟩ axis. The total accumulated ion charge per sample was always less

0163-1829/95/52(21)/15170(6)/$06.00 © 1995 The American Physical Society

than 3 μC. The concentrations of the displaced atoms were obtained by comparing the spectra from the virgin and damaged crystals with the random-oriented spectrum. The height of the random-oriented spectrum was verified by several measurements, obtained by aligning the sample to different angular orientations, well away from the ⟨100⟩ axis and from any planar channeling directions. The relative ion doses for different spectra were obtained by using a beam chopper with a separate pulse analysis system, which had an accuracy of better than 2%.

III. MOLECULAR-DYNAMICS SIMULATIONS OF THE RANGE PROFILES

The experimental range profiles were simulated using the molecular-dynamics (MD) method developed very recently at our laboratory.[15,22] The principles of the simulation algorithms are presented in detail in Ref. 23.

The starting position of the incident ^{30}Si atom was 5 Å above the surface of the computational cell of Si in the z direction, and was chosen randomly in the xy plane. The direction of the initial velocity of the incident ^{30}Si atom was aligned 6° from the normal of the surface of Si in the ⟨100⟩ direction. The end position of every incident atom was stored for the calculation of the range distribution. To estimate the distribution of primary damage the nuclear deposited energy was also calculated during the simulation runs.

Due to the high kinetic energies involved, periodic boundary conditions could not be applied. Instead, a slab of undisturbed silicon was generated in front of the incident atom every time it got close to the boundary of the computational cell. Thus the incident atom always moved in an undisturbed simulation cell.

The interatomic potential was taken from Ref. 15. For short internuclear separations ($r < 1.7$ Å), the potential was calculated through an accurate treatment of the interacting Si-Si dimer. The repulsive potential was then matched smoothly with the classical Stillinger-Weber many-atom potential,[24] which gives a good description of low-energy cohesion and bonding.

The short range repulsive potential was obtained from a self-consistent total energy calculation using density-functional theory and the local-density approximation (LDA) for electronic exchange and correlation.[25] The Kohn-Sham equations were solved numerically using a basis-set consisting of numerical atomic-type orbitals, and a discrete-variational method for the three-dimensional integrals.[26] The stability of the total energy results with respect to the basis set and the density of integration points was carefully monitored. The total energy, including both the electronic part and the internuclear Coulomb repulsion, was obtained as a function of the dimer distance, and defines the interatomic potential energy. In practice, we used the DMol package[27] well tested in calculations of energetics and structures of small molecules.

The experimentally confirmed electronic stopping power from Ref. 28 was included in the equations of motion of the incident atoms as a frictional force.[29]

IV. RESULTS AND DISCUSSION

A. Range distributions and crystallinity of the implanted samples

Figure 1 shows the ⟨100⟩ aligned backscattering spectra

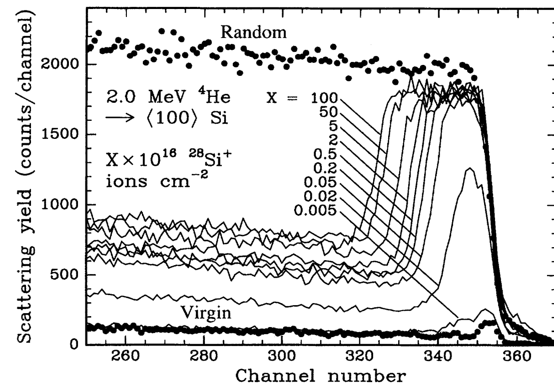

FIG. 1. RBS/channeling spectra for 2-MeV $^4He^+$ ions incident on the $5 \times 10^{13} - 1 \times 10^{18}$ 50-keV $^{28}Si^+$ ions cm^{-2} Si(100) samples. Also shown in the figure is the random-oriented spectrum and the spectrum in the ⟨100⟩ channeling direction for a virgin (unimplanted) sample.

for 2-MeV $^4He^+$ ions incident on the $5 \times 10^{13} - 1 \times 10^{18}$ 50-keV $^{28}Si^+$ cm^{-2} Si(100) samples. In the figure the damage induced by the $^{28}Si^+$ implantation is clearly visible as a difference between the spectra of the as-implanted and virgin Si samples. It is worth noting that the largest defect concentration does not reach the random level. The saturation of the number of displaced atoms is reached at the dose of 5×10^{14} $^{28}Si^+$ ions cm^{-2}. The backscattering yields are converted[30] to the displaced atom distributions in Fig. 2.

It can be seen that the width of the damaged region increases with dose. Figure 3 shows the full width at half maximum (FWHM) of the damaged region as a function of the implanted dose. In the figure the fitted logarithmic function

$$\mathrm{FWHM}\,(\mathrm{nm}) = a + b\,\ln[\mathrm{dose}\,(\mathrm{ions\ cm^{-2}})] \qquad (1)$$

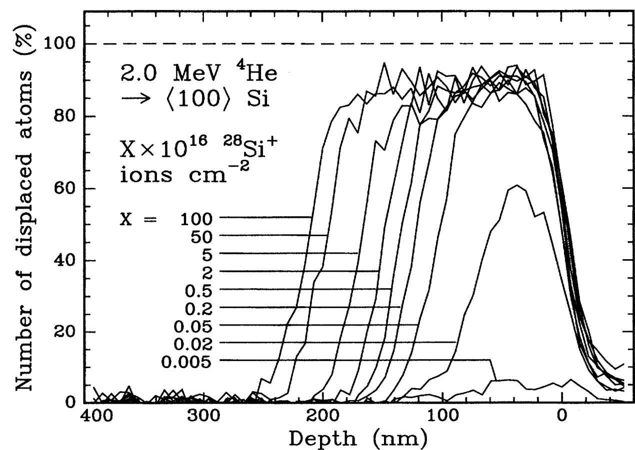

FIG. 2. Displaced atom distributions calculated from the RBS/channeling measurements. The dashed line indicates the random level.

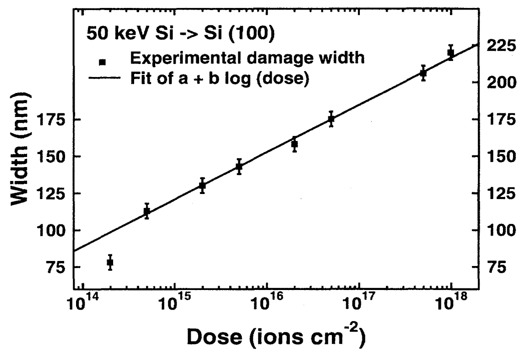

FIG. 3. Fit of Eq. (1) to the experimental damage width obtained with RBS/channeling measurements as a function of the implantation dose of ^{28}Si.

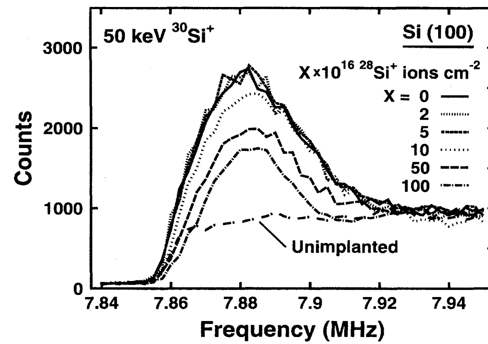

FIG. 4. NRB yields of the ^{30}Si$(p,\gamma)^{31}$P resonance reaction at E_p = 620 keV. The different curves indicate the amount of ^{28}Si implanted prior to the implantation of 2 × 10^{16} 50-keV ^{30}Si$^+$ ions cm^{-2}. Also shown is the measured natural concentration of ^{30}Si in unimplanted silicon. The square of the frequency given on the x axis is proportional to the beam energy.

illustrates the linear dependence of the FWHM on the logarithm of the dose. The values for a and b obtained in the fit were -357 ± 4 nm and 13.8 ± 0.2 nm, respectively.

An attempt to explain the observed linear dependence was made by assuming that "amorphization" of the silicon occurs when the concentration of implanted atoms or the deposited energy exceeds some threshold value. The exponential function

$$C(z)=c\ \exp(-z/d) \quad (2)$$

was fitted to the tail of the range or deposited energy curves (cf. Fig. 5). A good fit was obtained to both experimental and theoretical curves, giving values of d between 22 and 26 nm. If broadening of the damage region could be explained by the concentration of implanted atoms or deposited energy exceeding some threshold value, the coefficients b and d should have approximately the same value. Since this is not the case, a more complex damage creation procedure is involved.

Recent results indicate that mobile vacancies play an important role in the amorphization and recrystallization of c-Si.[7,16,31] This suggests that growth of the damaged layer is contributed to by migration of vacancies to the interface between the damaged region and c-Si and trapping there.

The ^{30}Si distributions measured with the NRB technique are shown in Fig. 4. The distribution is contributed to by the range distribution of ^{30}Si implants, the natural width of the resonance, the energy resolution of the proton beam, and the width of the energy-loss distribution for protons after traversing in c-Si. The enrichment of the isotope ^{28}Si in the sample due to the ^{28}Si implantation prior to the 2 × 10^{16} 50-keV ^{30}Si$^+$ ions cm^{-2} is seen in the reduction of the peak height caused by the reduction of the inherent amount of ^{30}Si.

By measuring the height of the edge of the implantation layer using a profilometer the sputtering coefficient was determined to be 0.9 ± 0.1, in a good agreement with the value of 0.8 obtained from experimental results and scaling laws in Ref. 32.

Range profiles where the decrease of the inherent amount of ^{30}Si has been taken into account, are shown in Fig. 5. It can be seen that the concentration distribution is not significantly affected by the increased damage produced along with the increased dose in the ^{28}Si implantations. The concentration of doped ^{30}Si atoms was obtained by comparison of the γ-ray yields from the doped ^{30}Si nuclei with those from isotope ^{30}Si in natural silicon. In the calculation of the depth scale, the stopping power of silicon for protons was taken from Ref. 33. The step in the excitation function arising from the natural ^{30}Si concentration was used in determining the zero point of the depth scale.

Literature results on damage produced in silicon self-ion-implantation in the 10–200 keV energy range contain some apparently contradictory results.[34] For instance, Holland *et al.*[10] and Kase *et al.*[19] report that silicon amorphizes at room temperature at a dose of about 5×10^{14} atoms cm^{-2}, while Prunier *et al.*[18] report that the temperature must be lower than 300 K to obtain amorphization. The differences in this case are probably due to differences in implantation dose rates and heat conduction conditions in the wafer holder. Also, we believe some confusion may result from the common practice to call structures where an RBS/channeling profile is close to the random level amorphous without doing a more detailed investigation of the actual structure. In fact

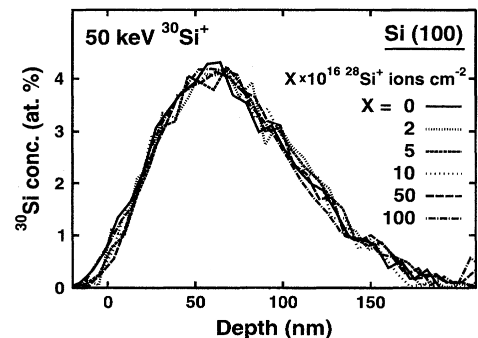

FIG. 5. Range distributions of ^{30}Si measured with the NRB technique. The different curves indicate the amount of ^{28}Si implanted prior to the implantation of 2 × 10^{16} ^{30}Si$^+$ ions cm^{-2}.

an RBS profile resembling the random spectrum may well result from for instance a polycrystalline sample structure.[11,35]

In general, there is fairly good agreement that silicon gets strongly damaged at a dose between 10^{14} and 10^{15} atoms cm^{-2} at room temperature,[6,10,19,36,37] in good agreement with our RBS results which show strong damage growth at a dose of 2×10^{14} atoms cm^{-2} (Fig. 2).

At higher implantation doses (close to or higher than 10^{16} atoms cm^{-2}), recrystallization is known to occur at temperatures higher than room temperature.[7,36,38–40] Some authors[10,36] have reported ion beam annealing at room temperature, but Cannavo *et al.* report that the beam annealing effect disappeared when a good thermal contact between the sample and the sample holder was employed during implantation.[36] Our implantations were performed with a sample holder which was in good thermal contact with the implanted samples, whence recrystallization effects were not to be expected.

Damage production is also known to be affected by the implantation dose rate (beam current). For otherwise equal implantation conditions the amount of damage grows[10,16] (or the recrystallization rate decreases[37]) with increasing dose rate. Holland *et al.* report that the onset of strong damage occurs at doses somewhat below 5×10^{14} atoms cm^{-2} in the dose rate range between 1 and 100 $\mu A\ cm^{-2}$, in good agreement with our RBS results.

B. X-ray and resistance measurements

The samples were also studied using x-ray facilities in the Physics department at the University of Helsinki. The (400), (422), and (311) reflections were measured for all the samples using a double-crystal diffractometer, Cu K_α-radiation, and nondispersive $(+,-)$ arrangement. The rocking curves were broader than the corresponding Darwin curves due to slightly dispersive geometry. Therefore, one unimplanted crystal was studied, too.

Each rocking curve had a higher tail than the reference curve at the low angle site and the magnitude of the tails increased with the implantation dose. The (400) rocking curves showed clearly stronger tails than the (422) and (311) rocking curves suggesting that the implantation generates stronger lateral than vertical strain fields. Thus the lattice spacing $\Delta d/d$ has changed more along the normal of the surface than along the plane of the surface. This agrees with other studies where lattice expansion or compression is observed.[9]

The resistivity of three implanted samples was determined using a two-point probe by measuring the resistance through the sample wafers at several different locations. For the samples implanted with 1×10^{18}, 4×10^{16}, and 5×10^{15} Si^+ ions cm^{-2} the measured resistivity of the damaged regions was $4\times10^{6}\ \Omega$ m, $3\times10^{6}\ \Omega$ m, and $0.7\times10^{6}\ \Omega$ m, respectively. In unimplanted parts of the sample the resistivity was about 5 Ω m.

The fact that implanted sample regions were found to have a roughly five to six orders of magnitude higher resistivity than unimplanted parts of the samples supports the conclusion that the sample structure is modified strongly at the beginning of the implantation, and that the structure is not sensitive to the implantation dose. The high resistivity indicates the presence of carrier traps, which may be related to vacancies in the interface between the damaged layer and *c*-Si (see above).

C. Range simulations for amorphous and crystalline structures

Due to the high implantation dose of 2×10^{16} $^{30}Si^+$ ions cm^{-2} practically all the implanted ions observable with the NRB method can be assumed to slow down in strongly damaged *c*-Si (cf. Fig. 2). In spite of the fact that the RBS/channeling measurements show that the implanted samples are neither crystalline (*c*-Si) nor amorphous silicon (*a*-Si), the range simulations were first carried out for *c*-Si and *a*-Si, which are typical approximations used in the literature in simulations of slowing down conditions. In simulating *a*-Si the initial coordinates of the lattice Si atoms were obtained from the 63 and 216 atom *ab initio* MD simulation cells described in Refs. 41–43.

In simulations of crystalline materials realistic thermal displacements of the atoms were obtained by simulating thermal movement at 300 K for 200 fs prior to the implantation simulations. Because the coordinates of the *a*-Si structure were taken from *ab initio* calculations it was not necessary to equilibrate the *a*-Si MD cell.

In every simulation run the trajectories of about 5000 incident ^{30}Si atoms were followed until they had slowed down to a cutoff energy of 1 eV.

For the comparison with the measured ^{30}Si distributions, the calculated range profiles were convoluted with the natural width of the resonance, the energy resolution of the proton beam, and the width of the energy-loss distribution for protons after traversing in Si. In the numerical convolution we used a Gaussian function which approximates well Vavilov's energy straggling distribution.[44,45] We have observed earlier[15] that the energy straggling of protons calculated according to the Bohr model[46] had to be multiplied by 0.9.

The simulated 50-keV and 100-keV ^{30}Si distributions are shown in Fig. 6 along with the experimental NRB results. The range profiles for amorphous silicon are fairly near a Gaussian profile, whereas the profiles for *c*-Si show a distinct tail due to channeling effects.

The comparison of the simulated range profiles with the experimental ones shows that the slowing down of Si ions has taken place in Si which is neither *c*-Si nor *a*-Si. The shapes of the experimental and simulated 100-keV range profiles are qualitatively very similar to their 50-keV counterparts, indicating that the implantation energy does not have a major effect on the final sample structure.

D. Range simulations for polycrystalline and other structures

Literature results indicate that silicon may reorder to a polycrystalline structure during very high-dose ($>10^{16}$ ions cm^{-2}) ion implantation.[11] The measured RBS/channeling results of our samples are similar to RBS spectra of polycrystalline silicon (poly-Si) reported in the literature.[9,35] The x-ray diffraction studies can be interpreted to indicate that the sample $\langle 100\rangle$ axis is close to that of bulk Si. The mea-

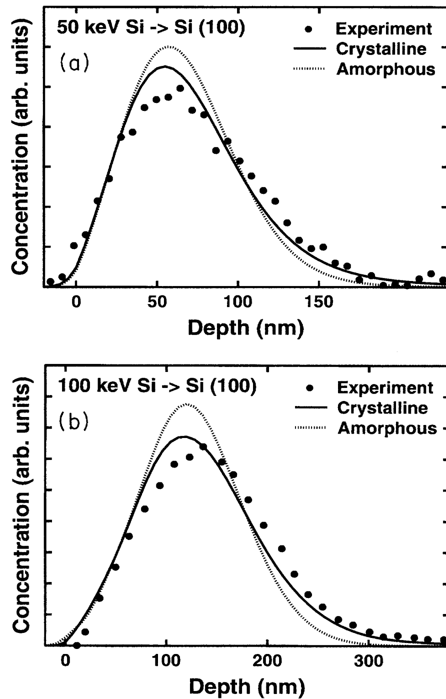

FIG. 6. Experimental and simulated range distributions for 50- (a) and 100-keV (b) Si self-ion implantation. The experimental distribution is the average of the three measured concentrations with the lowest amount of pre-implanted ^{28}Si. The simulated range results are for amorphous and crystalline silicon.

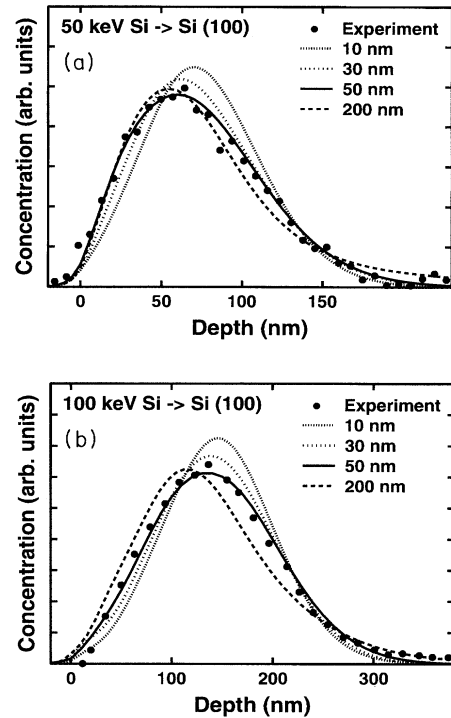

FIG. 7. Experimental and simulated range distributions for 50- (a) and 100-keV (b) Si self-ion implantation. The simulated range results are for polycrystalline silicon with domain sizes of 10, 30, 50, and 200 nm and random orientation between grains.

sured resistivities are in agreement with polycrystalline silicon, which is known to have a very much higher resistance than crystalline silicon.[47]

Since these experimental results are consistent with a polycrystalline sample structure, and since the range profiles obtained in MD simulations of a-Si and c-Si could not reproduce the NRB results, MD simulations were undertaken with different polycrystalline sample structures.

Polycrystallinity was modeled by selecting a grain size prior to the start of each simulation run. Average grain sizes ranging between 0.5 and 1000 nm were used. When the recoiling ion has traveled through each grain, it is injected into a new grain with the velocity it had when it left the former. The incident position of the ion entering in the new grain is selected randomly. The orientation of the new grain is either selected randomly or relative to the orientation of the previous grain. In the latter case the orientation of the $\langle 100 \rangle$ axis between grains is allowed to vary maximally some angle $\Delta\theta_{max}$.

Some simulated polycrystalline range profiles are shown in Fig. 7. For the profiles shown in the figure random orientation between adjacent grains was used. For small grain sizes the range profiles have an almost Gaussian form, similar to that of an amorphous profile. However, comparison of Fig. 6 and Fig. 7 shows that the front edge of the polycrystalline profile for a 10 nm grain size is significantly deeper in the sample than the amorphous profile. This can be attributed to the possibility of channeling in the first grains. For grain sizes larger than 30 nm the range profile has a visible tail at large z values, which can be readily understood to be due to the possibility of long-range channeling in the grains deep in the sample.

For grain sizes larger than about 30 nm the choice of the maximum angle between domains, $\Delta\theta_{max}$, was not found to affect the range distribution significantly. Both the 50 and the 100 keV experimental range distributions were well reproduced with a polycrystalline sample structure with domain sizes larger than 10 nm; see Fig. 7. The best fit was obtained with a grain size of 50 nm, regardless of the choice of $\Delta\theta_{max}$. If the orientation of the $\langle 100 \rangle$ axis of the first grain was selected to be less than about 7° deflected from the beam orientation, longer ranges were obtained due to channeling effects in the first grain.

Thus all the experimental and simulation results are consistent with a polycrystalline sample structure with an average grain size of roughly 50 nm, where the $\langle 100 \rangle$ axis of the grains deviates somewhat from the $\langle 100 \rangle$ axis of the bulk silicon underlying the damaged layer. This does not rule out the possibility that the damage is of a more complex character. An attempt to reproduce the experimental profile was made by simulating ranges in sample structures where parts of the structure was amorphous and other parts crystalline. No combination of amorphous-crystalline layers was found that reproduced well the experimental range profile.

V. CONCLUSIONS

In this work the effects of very high dose self-ion implantation on the structure of the implanted c-Si sample have

been studied using NRB and RBS/channeling measurements. A method for calculating ion ranges based on MD simulations was employed to analyze the experimental results. The effect of the sample structure on the simulated range profiles was examined.

The range measurements of 50-keV Si ions in c-Si by NRB and the crystallinity measurements of the samples by RBS/channeling over the dose range from 10^{13} to 10^{18} ions cm^{-2} show that the structure of the implanted sample does not change at doses 2×10^{16} to 10^{18} ions cm^{-2}. Range measurements of 100-keV Si ions showed that the ion energy is not a critical parameter with respect to the damage structure.

Furthermore, the experimental range results along with the MD simulations showed that the sample is strongly damaged but not amorphous and that the damaged region grows along with the amount of energy deposited in the implantations.

The range profiles obtained from MD simulations for a polycrystalline structure were sensitive to the grain size but not on the angle between the grain orientations. Simulated results along with the experimental profiles indicate a sample structure of polycrystalline silicon with a grain size of 50 nm.

ACKNOWLEDGMENTS

M. Hakovirta is acknowledged for performing the resistance measurements of the samples and Dr. V. Eteläniemi for administering the x-ray diffraction experiments. This work was supported by the Academy of Finland.

[1] G. D. Watkins, Phys. Soc. Jpn. (Suppl.) **II**, 22 (1963).
[2] L. J. Cheng, J. C. Corelli, J. W. Corbett, and G. D. Watkins, Phys. Rev. **152**, 761 (1966).
[3] M. L. Swanson, J. R. Parsons, and C. W. Haelke, in *Radiation Effects in Semiconductors 359*, edited by J. W. Corbetti and G. D. Watkins (Gordon and Breach, New York, 1971).
[4] S. Kurtin, G. A. Shifrin, and T. C. McGill, Appl. Phys. Lett. **14**, 223 (1969).
[5] V. S. Speriosu, B. M. Paine, M. A. Nicolet, and H. L. Glass, Appl. Phys. Lett. **40**, 604 (1982).
[6] T. Motooka and O. W. Holland, Appl. Phys. Lett. **58**, 2360 (1991).
[7] N. Hayashi *et al.*, Phys. Rev. Lett. **70**, 45 (1993).
[8] K. Saarinen *et al.*, Phys. Rev. B **43**, 4249 (1991).
[9] J. F. Knudsen *et al.*, Nucl. Instrum. Methods Phys. Res. B **59/60**, 1067 (1991).
[10] O. W. Holland, J. Narayan, and D. Fathy, Nucl. Instrum. Methods Phys. Res. B **7/8**, 243 (1985).
[11] C. E. Christodoulides *et al.*, Radiat. Eff. **36**, 73 (1978).
[12] P. L. F. Hemment *et al.*, Nucl. Instrum. Methods Phys. Res. B **209/210**, 157 (1983).
[13] S. T. Picraux, F. L. Vook, and H. J. Stein, in *Proceedings of the International Conference on Defects and Radiation Effects in Semiconductors,* Nice, France, 1978, edited by J. H. Albany (Institute of Physics, Bristol, England, 1979), p. 31.
[14] J. Mäkinen *et al.*, J. Appl. Phys. **67**, 990 (1990).
[15] J. Keinonen *et al.*, Nucl. Instrum. Methods Phys. Res. B **88**, 382 (1994).
[16] S. Tian *et al.*, J. Electrochem. Soc. (to be published).
[17] L. Sealy *et al.*, Nucl. Instrum. Methods Phys. Res. B **96**, 215 (1995).
[18] C. Prunier *et al.*, Nucl. Instrum. Methods Phys. Res. B **17**, 227 (1986).
[19] M. Kase, M. Kimura, H. Mori, and T. Ogawa, Appl. Phys. Lett. **56**, 1231 (1990).
[20] A. Kehrel *et al.*, Radiat. Eff. Def. **118**, 297 (1991).
[21] P. M. Endt and C. van der Leun, Nucl. Phys. **A310**, 1 (1978).
[22] P. Torri, J. Keinonen, and K. Nordlund, Nucl. Instrum. Methods Phys. Res. B **84**, 105 (1994).
[23] K. Nordlund, Comp. Mat. Sci. **3**, 448 (1995).
[24] F. H. Stillinger and T. A. Weber, Phys. Rev. B **31**, 5262 (1985).
[25] R. Jones and O. Gunnarsson, Rev. Mod. Phys. **61**, 689 (1989).
[26] J. Delley, J. Chem. Phys. **92**, 508 (1990).
[27] DMol is a trademark of Bio Sym. Inc., San Diego, California.
[28] J. Keinonen, K. Arstila, and P. Tikkanen, Appl. Phys. Lett. **60**, 228 (1992).
[29] A. Kuronen *et al.*, Nucl. Phys. **A549**, 59 (1992).
[30] L. C. Feldman, J. W. Mayer, and S. T. Picraux, *Materials Analysis by Ion Channeling* (Academic, New York, 1982).
[31] N. Hayashi *et al.*, Nucl. Instrum. Methods Phys. Res. B **80/81**, 1006 (1993).
[32] *Sputtering by Particle Bombardment I*, edited by R. Behrisch (Springer, Berlin, 1981).
[33] H. H. Andersen and J. F. Ziegler, *The Stopping and Range of Ions in Matter* (Pergamon, New York, 1977), Vol. 3.
[34] R. B. Simonton, Nucl. Instrum. Methods Phys. Res. B **21**, 490 (1987).
[35] J. D. Williams and P. Ashburn, J. Appl. Phys **72**, 3169 (1992).
[36] S. Cannavò *et al.*, Appl. Phys. Lett. **47**, 138 (1985).
[37] J. Linnros and G. Holmén, J. Appl. Phys. **62**, 4737 (1987).
[38] H. Sayama, A. Kinomura, Y. Yuba, and M. Takai, Nucl. Instrum. Methods Phys. Res. B **80/81**, 587 (1993).
[39] K. Kuriyama *et al.*, Nucl. Instrum. Methods Phys. Res. B **80/81**, 994 (1993).
[40] J. S. Williams, R. D. Goldberg, M. Petravic, and Z. Rao, Nucl. Instrum. Methods Phys. Res. B **84**, 199 (1994).
[41] D. A. Drabold, P. A. Fedders, O. F. Sankey, and J. D. Dow, Phys. Rev. B **42**, 5135 (1990).
[42] P. A. Fedders, D. A. Drabold, and S. Klemm, Phys. Rev. B **45**, 4048 (1992).
[43] D. A. Drabold (private communication).
[44] J. Keinonen, M. Hautala, I. Koponen, and M. Erola, Phys. Rev. B **41**, 9907 (1990).
[45] P. V. Vavilov, Zh. Éksp. Teor. Fiz. **32**, 920 (1957) [Sov. Phys. JETP **5**, 749 (1957)].
[46] N. Bohr, Mat. Fys. Medd. Dan. Vid. Selsk. **18**, 8 (1948).
[47] S. M. Sze, *Semiconductor Devices, Physics and Technology* (John Wiley & Sons, New York, 1985).